Journal of Alloys and Compounds 855 (2021) 157431

Contents lists available at ScienceDirect

Journal of Alloys and Compounds

journal homepage: http://www.elsevier.com/locate/jalcom

Comparing amorphous silicon prepared by electron-beam evaporation and sputtering toward eliminating atomic tunneling states

Xiao Liu [a, *], Matthew R. Abernathy [a, 1], Thomas H. Metcalf [a], Battogtokh Jugdersuren [b], James C. Culbertson [a], Manel Molina-Ruiz [c], Frances Hellman [c]

[a] Naval Research Laboratory, Code 7130, Washington, D.C., 20375, USA
[b] Jacobs Engineering Group, Hanover, MD, 21076, USA
[c] Department of Physics, University of California Berkeley, Berkeley, CA, 94720, USA

ARTICLE INFO

Article history:
Received 17 August 2020
Received in revised form
29 September 2020
Accepted 30 September 2020
Available online 3 October 2020

Keywords:
Amorphous materials
Thin films
Reactive sputtering
Quantum tunneling
Acoustic properties
Rutherford backscattering

ABSTRACT

It has previously been shown that amorphous silicon (*a*-Si) thin films can be produced free of tunneling two-level systems (TLS) by *e*-beam evaporation onto substrates held at elevated temperatures, and there appears to be a strong anticorrelation between the atomic density of these films and the number density of TLS. We have prepared *a*-Si films with higher atomic density using magnetron sputtering at substrate temperatures comparable to those used in the *e*-beam studies. We compare the atomic densities measured using Rutherford backscattering and the shear moduli, the speeds of sound, and the densities of TLS calculated using internal friction measurements at cryogenic temperatures of sputtered *a*-Si films to those of the *e*-beam films. Our results show that despite their higher atomic densities, sputtered *a*-Si films prepared at elevated substrate temperatures have lower speeds of sound and higher densities of TLS, which we attribute to the different film growth mechanism from that of *e*-beam evaporation. We conclude that a collaborative improvement of both local structure and network connectivity, determined by atomic density and speed of sound, respectively, to approach their crystalline values is required to eliminate atomic tunneling states.

Published by Elsevier B.V.

1. Introduction

Amorphous solids are known for their ubiquitous low-energy excitations that make them differ from their crystalline counterparts in a variety of low temperature properties [1,2]. These low-energy excitations contribute to an anomalously large and linear temperature (T) dependent specific heat and their resonant scattering of phonons leads to a T^2 dependent thermal conductivity, both at $T < 1$ K [3]. These phenomena have been explained by the model of tunneling two-level systems (TLS), where an atom or a cluster of atoms tunnel between two adjacent potential minima in the amorphous structure when the wave function of the states overlap [4,5].

The two-level nature of such excitations results in resonant scattering [6–8], saturations [9,10], and echoes [11] of acoustic and electromagnetic waves. These effects are typically observed at $T < 100$ mK. The relaxation scattering of external elastic waves results in a nearly T independent plateau in internal friction at 0.5–10 K, depending on the external acoustic frequency [12,13] given by

$$Q_0^{-1} = \frac{\pi}{2} C, \tag{1}$$

where the tunneling strength C is defined as

$$C = \frac{\overline{P}\gamma^2}{\rho v^2}, \tag{2}$$

and $\overline{P}$ is the spectral density of the tunneling states, γ their phonon coupling energy, ρ the mass density, and v the speed of sound. With increasing temperature tunneling gives way to thermal activation showing a broad maximum in internal friction after the plateau. Within the same temperature range, the relative change of speed of sound decreases first logarithmically, then linearly from a few K up to a few tens of K, also depending on the

* Corresponding author.
E-mail address: xiao.liu@nrl.navy.mil (X. Liu).
[1] Current address:The Johns Hopkins University, Applied Physics Laboratory, Laurel, MD, 20723, USA.

https://doi.org/10.1016/j.jallcom.2020.157431
0925-8388/Published by Elsevier B.V.

external acoustic frequency [14] as:

$$\Delta v / v_0 = -\beta(T - T_0), \quad (3)$$

where v_0 is the speed of sound at a reference temperature T_0 and β is proportional to C for most amorphous and disordered crystalline solids studied so far [15]. The loss maximum and the linear decrease of $\Delta v/v_0$ are understood as the thermally activated relaxation rate dominating the quantum tunneling rate of the TLS [14,16].

Despite the success of the TLS model, a number of questions remain unanswered: what are the tunneling entities, and why are the properties so universal? In particular, $10^{-4} \leq C \leq 10^{-3}$ is found for most of the amorphous solids, including some disordered crystalline solids and complex crystals with diverse structures and compositions, even as the individual parameters, such as pv^2, can vary by as much as five orders of magnitude [17].

The universal nature of TLS confounds the identification of their origin. That's why exceptions are particularly valuable. An early internal friction study of hydrogenated amorphous silicon (*a*-Si) films deposited at an elevated substrate temperature shows a more than two orders of magnitude reduction of C [18]. However, the right amount of hydrogen was thought to be the main reason [19]. A recent study of *e*-beam evaporated *a*-Si utilizing both specific heat and internal friction measurements showed that elevated substrate temperatures during deposition are the overriding cause of low TLS densities in these films, without the need for hydrogen [20,21]. It has been known that vapor deposition at a substrate temperature T_{sub} slightly below its glass transition T_g where freshly landed atoms have enough mobility to equilibrate in a stable and low energy state results into a densely packed structure that is close to an ultrastable state of glasses [22]. A specific heat study shows that a stable glassy polymer material—indomethacin deposited at $T_{sub} \approx 0.85T_g$ has a much smaller TLS density than its conventional form cooled from glass transition [23].

In a quantitative analysis of *e*-beam *a*-Si, it is evident that the TLS density decreases exponentially with increasing atomic density [24]. In *e*-beam *a*-Si, a high atomic density is a result of an elevated substrate temperature. However, it is known that high atomic density can also be accomplished by sputtering. In this work, we study magnetron sputtered *a*-Si films in order to achieve higher atomic density in *a*-Si and to differentiate its relative importance from high substrate temperatures. There is also a historic incentive to study TLS in sputtered *a*-Si that relates to their microscopic origin. Although the TLS model was proposed purely phenomenologically, Phillips suggested in his original theory work that TLS would occur in an open structure with low atomic bonding, but not in a closed one with tetrahedral bonding like *a*-Si and *a*-Ge [5]. Due to technical challenges in studying TLS in thin films, no decisive conclusions have been drawn in early studies [25–27]. Later on, a double-paddle oscillator (DPO) study confirmed the existence of TLS in both *a*-Si and *a*-Ge, and their tunneling strength C are smaller than most other amorphous solids [28]. Encouragingly, C in room temperature (RT) sputtered *a*-Si is found to be lower than in *e*-beam, and decreases by a larger percentage after an anneal at 350°C [28]. A comparison of T_{sub} dependence of *e*-beam and sputtered *a*-Si with the known difference in atomic density will give us more insight into a more effective route to eliminate TLS. Amorphous thin films devoid of TLS would untangle a plethora of current challenges in technological areas, such as superconducting quantum bits [29] and the next generation gravitational-wave detectors [30].

To facilitate the comparison, thin films of *a*-Si are sputtered at RT, 303°C, 370°C, and 431°C. The same DPO technique as we used previously on *e*-beam *a*-Si films is used to measure C of TLS. Our results do not support the determinative effect of atomic density on the density of TLS, rather the formation of tunneling states may depend on the microscopic details of film deposition and growth processes.

2. Experimental

Four *a*-Si thin films were prepared in this work with a substrate temperature during growth between 30°C and 431°C. They were deposited onto a single crystal DPO with an AJA magnetron sputtering system using a 5 N 2" Si target at a target-to-substrate working distance of 77 cm. For all depositions, two pieces of witness substrates, one single crystal silicon and one single crystal sapphire, were co-deposited, which were later used for Raman spectroscopy and Rutherford backscattering spectrometry (RBS) measurements, respectively. Prior to deposition, the system was evacuated to a base pressure below 10^{-7} Torr except for the RT film where the base pressure was 4×10^{-7} Torr. Deposition processes started with a 3–5 min back-sputtering with 10 W DC power to clean substrates. This was followed by a 5 min pre-sputter to remove oxide and nitride from the surface of the target and to further reduce residual oxygen in the deposition chamber before opening the shutter for deposition. RF power was used for pre-sputter and sputter with a power of 100 W for the 303°C and 370°C films and 150 W for the RT and 431°C films. All depositions lasted ~ 3 hours (6 h for the 303°C film). During deposition of the 431°C film, RF power became unstable after about 80 min, restarted at 200 W for 30 min, and subsequently reduced back to 150 W for the remaining time. Argon gas flow was maintained at 25 sccm throughout for all films, except 10 sccm for the 370°C film, and its partial pressure at 20 mTorr during back-sputter and 3 mTorr during pre-sputter and sputter.

Raman spectroscopy measurements performed on films deposited on silicon witness substrates confirm all four films were amorphous. In addition, we find that a sign of crystallinity starts to appear when the substrate temperature is raised to 451°C. RBS measurements were conducted to determine the atomic density and composition using the films deposited on sapphire witness substrates. All films show the same 0.5 at.% argon which is homogeneously distributed throughout the films, typical for sputtered films. Only the RT film shows about 2–3 at.% oxygen through the film with increasing oxygen content toward the substrate. This may be attributed to the higher base pressure than the others. No signs of oxygen are found inside the three films grown at elevated substrate temperatures within an error of 0.5% except for some 4–5 nm thick native oxide at their surfaces. Film thicknesses were measured with an N&K Spectrophotometer in reflection mode at Naval Research Laboratory and with a KLA-Tencor Alpha-Step IQ Surface Profilometer at UC Berkeley on both types of witness substrates. The results are within 3% for most. Due to the small oxygen content in the RT film, the optically determined thickness does not appear reasonable. We choose the profilometry thickness instead. By considering the possible thickness variations between DPOs and witness substrates, we find a thickness error bar of 5% is appropriate for our analysis of elastic properties. Overall, excluding argon and oxygen, sputtering results in higher atomic density n_{Si} than by *e*-beam evaporation and the n_{Si} increases with T_{sub} at a much slower pace [20]. The thicknesses and atomic densities are listed in Table 1.

The DPOs are fabricated into the shape shown in the inset of Fig. 1 (a) using an undoped or lightly n-type doped single crystal silicon wafer, 300 μm thick [31]. They consist of a head, a neck, two wings, a leg and a foot. They are mounted by clamping the bottom half of their foot to an invar block with a precision torque wrench, which is then mounted in a He3 cryostat. The activation and

Table 1
PECVD *nc*-Si film names, parameters, and thermal conductivity at 300 K.

T_s (°C)	thickness (nm)	dep rate (nm/s)	$n_{Si} \times 10^{22}$ (1/cm^3)	G (GPa)	$v_t \times 10^3$ (m/s)	$Q_0^{-1} \times 10^{-5}$	$\overline{P}\gamma^2 \times 10^6$ (J/m^3)	$\overline{P} \times 10^{44}$ (1/Jm^3)
RT	301	0.028	4.93±0.10	38.5	4.09	4.97	1.27	3.8
303	327	0.015	4.94±0.12	46.4	4.49	2.87	0.84	2.5
370	265	0.025	4.95±0.12	51.3	4.71	1.69	0.55	1.9
431	218	0.026	4.98±0.13	52.7	4.76	1.41	0.48	1.4

detection of a resonance mode are achieved capacitively with a 3 nm-Ti/50 nm-Au coating on its wings. We use the so-called antisymmetric mode at ~ 6000 Hz, in which the head and the wings vibrate out of phase, and thus twist the neck into a torsional oscillation. Due to its excellent vibration isolation, the antisymmetric mode has a narrow resonant width of its frequency and low background internal friction ($\sim 2 \times 10^{-8}$). The addition of a film on the neck leads to a measurable shift of its resonance frequency $\Delta f = f_{sub} - f_{osc}$, and internal friction $\Delta Q = Q_{sub}^{-1} - Q_{osc}^{-1}$. The temperature dependence of shear modulus G_{film}, internal friction Q_{film}^{-1}, and relative change of speed of sound $(\Delta v/v_0)_{film} = [v_{film}(T) - v_{film}(T_0)]/v_{film}$ of the films can be calculated through [31]:

$$G_{film} = \frac{2G_{sub}t_{sub}}{3t_{film}}\frac{\Delta f}{f_{sub}}, \tag{4}$$

$$Q_{film}^{-1} = \Delta Q\frac{f_{sub}}{2\Delta f} + Q_{sub}^{-1}, \tag{5}$$

$$\left(\frac{\Delta v}{v_0}\right)_{film} = \left[\left(\frac{\delta f}{f_0}\right)_{osc} - \left(\frac{\delta f}{f_0}\right)_{sub}\right]\frac{f_{sub}}{2\Delta f} + \left(\frac{\Delta v}{v_0}\right)_{sub} \tag{6}$$

where t, G, and $\delta f/f_0 = [f(T) - f(T_0)]/f(T_0)$ are thicknesses, shear moduli, and relative changes of resonance frequency, respectively, of the oscillators, the substrates, and the films. T_0 is a reference temperature taken as the lowest temperature point of the experiment. For the single crystal Si along ⟨110⟩ we have $G_{sub} = 62$ GPa and $t_{sub} = 300$ μm.

3. Results

The internal friction results of the DPOs, Q_{osc}^{-1}, carrying the four sputtered *a*-Si films with $T_{sub} = 30^\circ$ (RT), 303°C, 370°C, and 431°C are shown in Fig. 1(a). The inset shows a photograph of a real DPO carrying a film on its neck area and a metal coating on its wings that extends to its leg and the foot. The background internal friction Q_{sub}^{-1} was measured separately for each of the DPOs and a typical one is shown as the solid line. The value of the background loss, depending weakly on the actual size of the DPO which is determined by the details of fabrication, is close to 10^{-8} below 30 K and is thought to originate from some surface losses and attachment loss [32]; the rise above 30 K follows thermoelastic loss of silicon up to room temperature [33].

The calculated results of the sputtered *a*-Si films, Q_{film}^{-1}, using Eq. (5) are shown in Fig. 1(b). For a comparison with a prototypical amorphous solid, Q_{film}^{-1} of a 107 nm thick dry thermal oxide (*a*-SiO_2) film grown directly on a DPO at 1100°C is shown as a solid line. Selected data of *e*-beam *a*-Si with $T_{sub} = 45$, 200, 350, and 400°C are also shown for comparison. Two observation can be made. First, like *e*-beam *a*-Si films, the sputtered *a*-Si films have a temperature-independent plateau below 10 K that relates to C by Eq. (1) and it increases to develop a broad maximum at 160–170 K. The height of the maximum appears to be proportional to the value of its plateau for both *e*-beam and sputtered *a*-Si films for a variation over one order of magnitude. The maximum becomes invisible within the experimental resolution as the plateau drops into the range of 10^{-6}

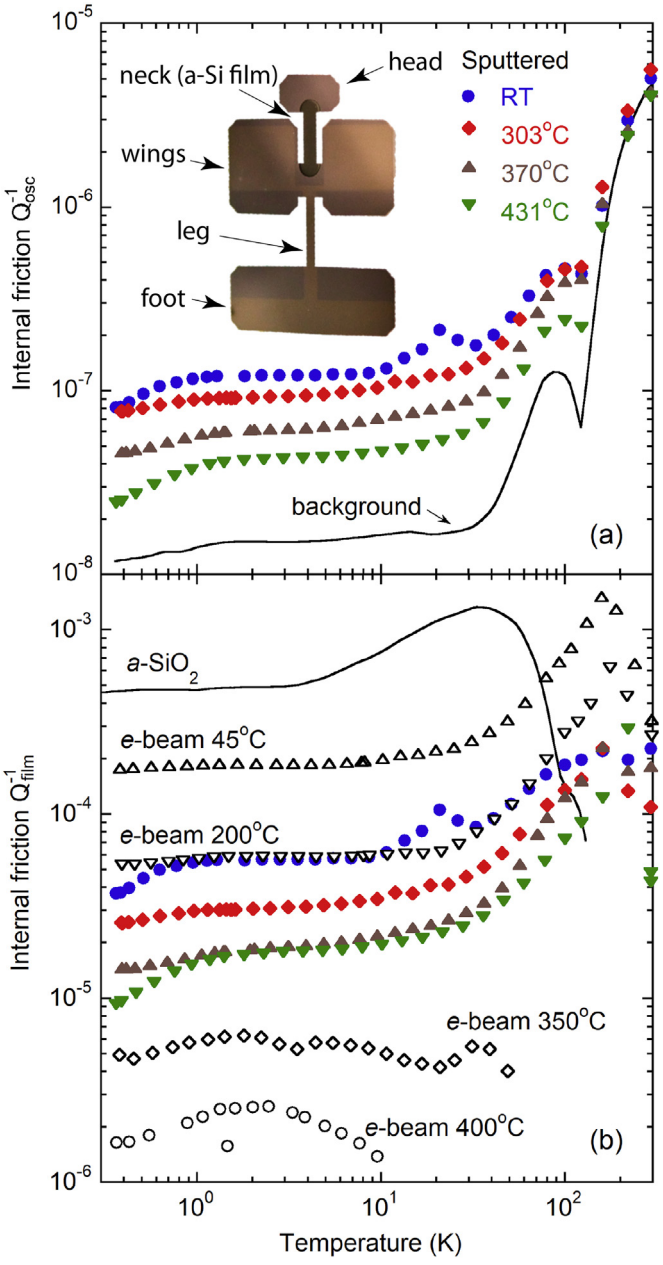

Fig. 1. (a) Temperature dependence of Q_{osc}^{-1} of four DPOs carrying the sputtered *a*-Si deposited at RT, 303°C, 370°C, and 431°C. The solid line is a representative DPO background without a film. The inset is a photograph of a real DPO carrying a film on the neck area and a metal coating on its wings, leg and bottom half of the foot. (b) Temperature dependence of the four sputtered *a*-Si. Data of selected *e*-beam *a*-Si with T_{sub} labelled, and a 107 nm thick dry thermal oxide of silicon (*a*-SiO_2) as a solid line, both of which are from Ref. [21], are shown for comparison.

for *e*-beam films with $T_{sub} \geq 350^{\circ}C$. This result supports the common structural origin of the TLS and the excitations for thermal activation [13]. Note that a small peak at 20 K in the RT sputtered film is seen, but is not reproduced in other RT trials and is likely an experimental artifact. Second, although the values of the Q_0^{-1} at RT is about a factor of 4 smaller than in *e*-beam in good agreement with earlier studies [28], Q_0^{-1} of sputtered *a*-Si only decreases by a factor of 3.5 from RT to $T_{sub} = 431^{\circ}C$; the same amount of reduction has been achieved by an anneal at 350°C of an RT film [28]. In contrast, a drop of two orders of magnitude in Q_0^{-1} has been observed in *e*-beam *a*-Si from RT to $T_{sub} = 400^{\circ}C$. As a result, the lowest TLS density in sputtered *a*-Si films is about one order of magnitude higher than in *e*-beam films despite the fact that all sputtered films have higher atomic densities and start with a significantly lower C for the film grown at RT.

The change of C with T_{sub} can also be observed in the change of speed of sound for temperature below 20 K, where a linear decrease of $\Delta v/v$ with T following Eq. (3) dominates as shown in Fig. 2. The results of the same *a*-SiO_2 film and *e*-beam *a*-Si films with $T_{sub} =$ 45 and 400°C as shown in Fig. 1(b) are provided for comparison. The narrower range of the slopes, β, nicely mirrors the narrower range of the plateaus in internal friction for sputtered *a*-Si than in *e*-beam, which is consistent with Eq. (3). Put together, both internal friction and the change of sound speed consistently show that a sizable amount of TLS remain in sputtered *a*-Si despite the elevated substrate temperatures. We can thus conclude that the elevated substrate-temperature approach that is extremely successful in *e*-beam *a*-Si films is not as effective at reducing the density of TLS in magnetron sputtered *a*-Si films.

We notice a maximum in $\Delta v/v$ at $\sim$ 1 K for the RT and 431°C films and a corresponding decrease of Q^{-1} at the same temperature. These may look like an end of relaxation process when the TLS relaxation rate lags the acoustic frequency with decreasing temperature. However, such a transition has been observed at 0.1 K in a recent low temperature DPO measurement of an *e*-beam *a*-Si film with a similar frequency [34]. While we are continuing to search for the source of this anomaly, we would not consider it for our analysis for the time being as it would not affect the results of this work.

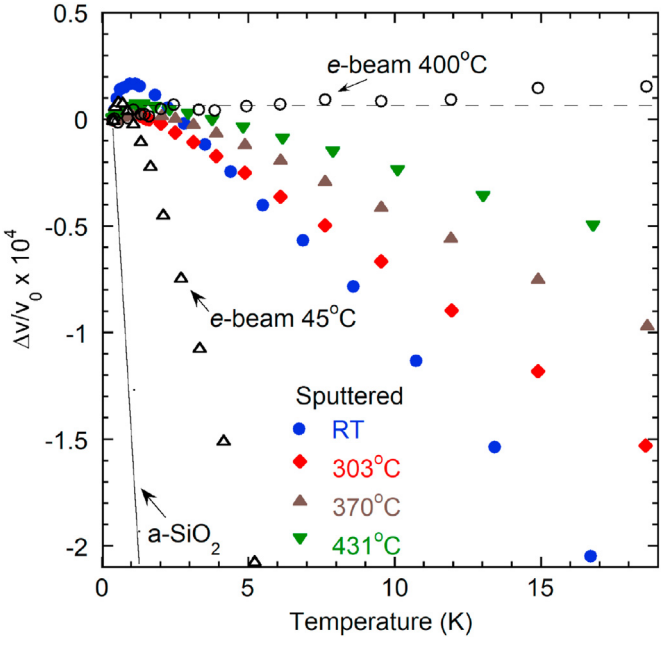

Fig. 2. Temperature dependent $\Delta v/v_0$ of the four sputtered *a*-Si films, two *e*-beam *a*-Si with $T_{sub} = 45^{\circ}$ and 400°, and a 107 nm thick dry thermal oxide of silicon (*a*-SiO_2) as a solid line, both of which are from Ref. [21]. The horizontal dashed line represents zero slope of β.

To put the above results in perspective, we show in Fig. 3 the structure parameters, n_{Si}, G, and v_t in (a)-(c), and TLS parameters, Q_0^{-1}, $\overline{P}\gamma^2$, and $\overline{P}$ in (d)-(f) as a function of T_{sub}. We determine the low temperature shear modulus G using Eq. (4), and with that, we calculate the transverse speed of sound of the sputtered *a*-Si films $v_t = \sqrt{G/\rho}$ and $\overline{P}\gamma^2$ of TLS (Eq. (2)). In order to compare with specific heat results of *e*-beam *a*-Si, we need to separate $\overline{P}$ from γ, which has not been determined for sputtered *a*-Si films as far as we know. As we have used $\gamma = 0.36$ eV before to compare specific heat and internal friction of *e*-beam *a*-Si [24], we continue to use the same value for sputtered *a*-Si to estimate $\overline{P}$ in this work for the ease of comparison. Note that γ of a RT *e*-beam *a*-Si has recently been determined to be $\gamma \approx 1$ eV [34]. The choice of γ shifts the ratio of $\overline{P}$ estimated from specific heat and internal friction and has no impact to our conclusions. The results are also given in Table 1.

Fig. 3(a) shows atomic densities of all sputtered *a*-Si films are higher than in *e*-beam films. The density deficit relative to crystalline silicon (*c*-Si) decreases from 1.3% to 0.3% with increasing T_{sub}. These densities are among the highest in *a*-Si, similar to those of amorphized *c*-Si formed by ion implantation [36]. The density difference from the *e*-beam films is the largest at RT, where Q_0^{-1} in sputtered *a*-Si is four times smaller. This result underscores the importance of atomic density on the TLS [24]. However, at the highest T_{sub}, Q_0^{-1} in sputtered *a*-Si is more than five times larger. In contrast to n_{Si}, Fig. 3(c) shows that sputtering does not systematically increase the speeds of sound. At RT, we find the values of v_t are roughly the same for both *e*-beam and sputtered films, which are about 78% of polycrystalline silicon [35]. These values are consistent with the reported ones, where *e*-beam and sputtered films have speeds of sound 77% [37] and 71% [38] of the poly-Si value, respectively. The most important observation in Fig. 3(a)–(c) is that T_{sub} affects *e*-beam films more than sputtered films in all structural properties as n_{Si}, G, and v_t all increase faster toward their corresponding crystalline values in *e*-beam films than in sputtered films. As a result, although G starts higher in sputtered films at RT, it becomes lower than that of *e*-beam at the highest T_{sub}. This trend continues in all TLS parameters shown in Fig. 3(d)–(f). It is likely that sputtering is effective in densely packing silicon atoms much more than *e*-beam evaporation. However, such packing pushes adatoms into undesirable high energy states with broken bonds, thus increasing atomic density without improving network connectivity in terms of G and v_t and that compromises the effect of elevated substrate temperatures.

In Fig. 3(f), a few data points converted from specific heat measurements are included for comparison [20]. Specific heat measures TLS density n_0 which is obtained from the linear T-term observed at low temperatures. Following the TLS model, $n_0 = \overline{P}/2\ln(4\tau/\tau_{min})$, where τ and τ_{min} are the measurement time and the minimum relaxation time of TLS, respectively. Like in Ref. 70 where a comparison between internal friction and specific heat measurements have been made, we assume $\overline{P} = n_0/8$. The important point to make here is that at $T_{sub} = 45$ and 200°C values of $\overline{P}$ spreading by as much as a factor of eight have been observed. The variation in these values at a constant T_{sub} is a result of an unexpected dependence upon film thickness. However, such thickness dependence is absent in v_t for the samples studied in that work. In other words, despite the dominating effect of T_{sub}, *e*-beam *a*-Si films with smaller thicknesses would have a local structure that reduces their atomic densities and increases the density of TLS without affecting their speeds of sound [39]. In sputtered *a*-Si films,

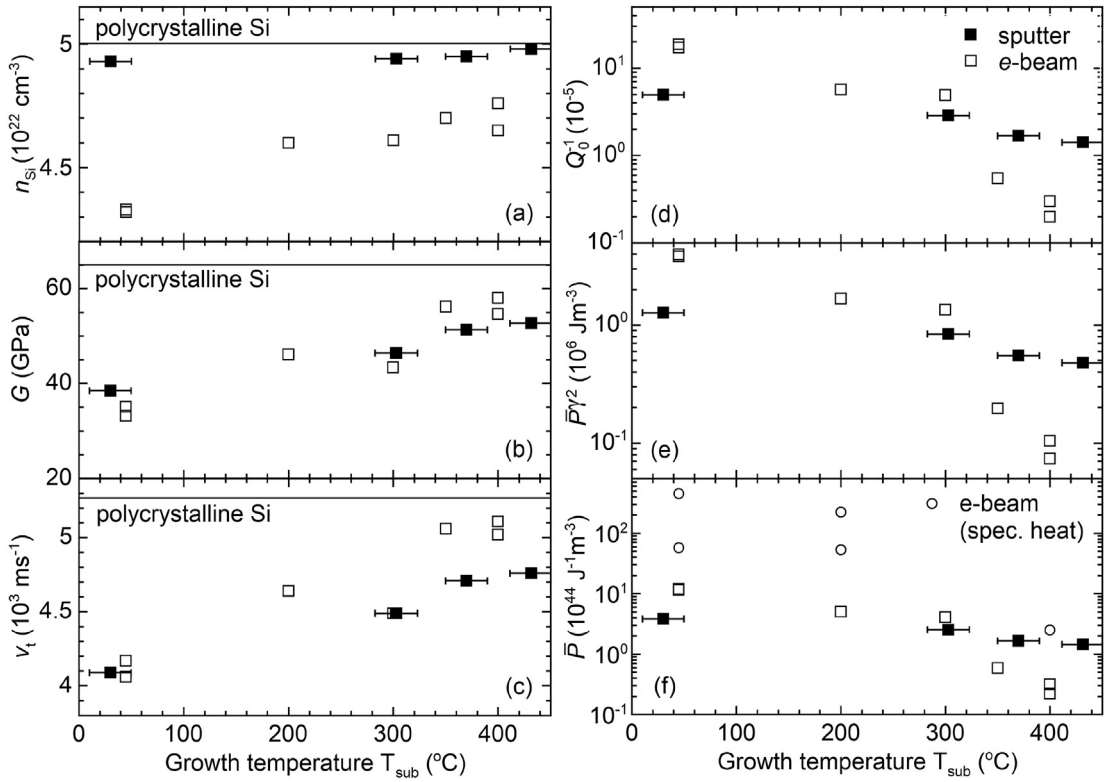

Fig. 3. Growth temperature dependence of atomic density n_{Si}, shear modulus G, transverse speed of sound v_t, internal friction plateau Q_0^{-1}, and TLS parameters $\bar{P}\gamma^2$, and $\bar{P}$ from (a) to (f) in the order listed. $\gamma = 0.36$ eV is used to estimate $\bar{P}$. Sputtered a-Si data of this work are shown as closed squares with error bars. Data of e-beam a-Si from DPO measurements [21] and specific heat measurements [20] are shown as open squares and open circles, respectively. The horizontal lines in (a)–(c) represent values of polycrystalline silicon [35].

however, although the atomic densities are higher, the lack of improvement in speeds of sound hinders the reduction of TLS density. The comparison between e-beam and sputtered a-Si films demonstrates that both atomic density and speeds of sound are independently tunable and a collaborative improvement of both to approach their crystalline values is required to eliminate TLS.

4. Discussions

That Q_0^{-1} in the sputtered films is significantly larger than in e-beam films at elevated T_{sub} suggests an incompletely-understood dependence of either $\bar{P}$ or γ on growth conditions, and is similar to what was found in hydrogenated a-Si [39,40], where a similar Q_0^{-1} was found along with a very high density of TLS from specific heat. There, the mechanism has been suggested to be related to the presence of H (in the form of Si–H bonds) in lower density areas resulting in high n_0 and low γ.

Having realized that T_{sub} is not as determinative of TLS as we previously thought, we show v_t and $\bar{P}$ as a function of n_{Si} in Fig. 4. With increasing n_{Si}, we see v_t increases and $\bar{P}$ decreases concomitantly for both e-beam and sputtered films as expected. However, the lack of correlation in n_{Si} dependence of both v_t and $\bar{P}$ between these two deposition methods suggests that different film growth mechanisms may be in play. For e-beam evaporation, deposited atoms have little extra kinetic energy by themselves to diffuse on the unheated surface, resulting in nanovoids and low density regions that are typical for e-beam a-Si as revealed by transmission electron microscopy [24]. A high substrate temperature and a slow deposition rate would facilitate surface diffusion of freshly deposited adatoms to find low energy positions leading to a denser and

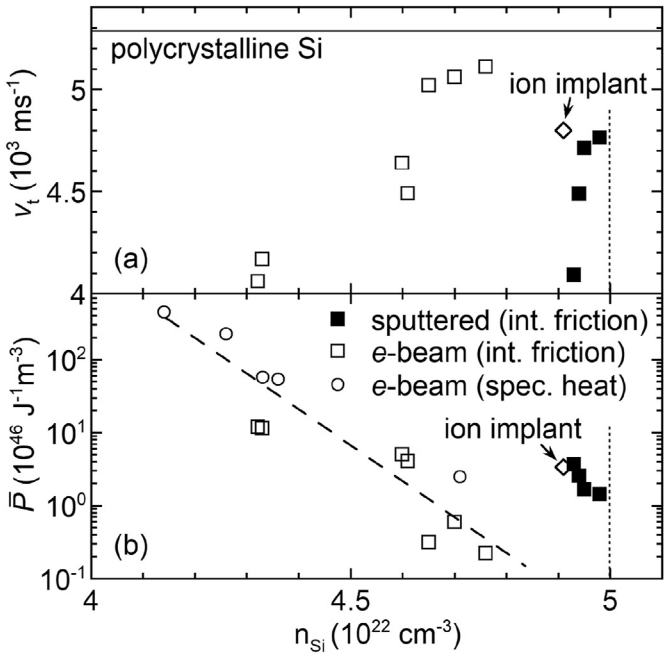

Fig. 4. Silicon atomic density dependence of transverse speed of sound v_t (a) and spectral density $\bar{P}$ (b). $\gamma = 0.36$ eV is used to estimate $\bar{P}$. The symbols have the same meaning as in Fig. 3. Data point of amorphized silicon by ion implantation are from: (a), 84; and (b), 74. The dotted vertical lines in both (a) and (b) are n_{Si} value of crystalline Si. The horizontal line in (a) represents v_t of polycrystalline silicon. The dashed line is a guide to the eye only.

more ordered network structure, similar to the process that makes vapor deposited molecules ultrastable [41]. For sputtering, the ions/atoms are deposited with energies as much as 100 times higher than those of the evaporated atoms, a process known as atomic peening. As a result, some deposited ions/atoms can be driven into spaces that are otherwise too small under normal thermodynamic equilibrium conditions including interstitial sites [42]. Although the higher kinetic energy also raises the substrate temperature and promotes the surface mobility, the disruptions and displacements by the continued impingement of ions/atoms overwhelm any diffusion process. Although this leads to higher atomic density than in *e*-beam, more atoms are left in higher energy positions with unconnected bonds. This is evident from the observation that the data points of an *a*-Si film amorphized by ion implantation, also shown in Fig. 4(a) and (b) where its n_{Si}, v_t, and $\overline{P}$ are taken from Refs. 82, 84, and 74, respectively, are in the same vicinity of sputtered *a*-Si. The implanted ions carry even higher energy than in sputtering. For *e*-beam evaporation, the effect of elevated T_{sub} is to reduce voids and to improve network connectivity through enhanced surface diffusion; that's why T_{sub} is much more effective at improving the structural properties and reducing the TLS density. Contrarily, for sputtering the effect of elevated T_{sub} may act more to relax intrinsic strain accumulated during sputtering than to enhance surface mobility; that's why its effect on the structural properties is weak, and its effect on the TLS density is similar to a post-deposition anneal [28].

Our results can be compared with those of ion-beam sputtered *a*-Si films [43–45]. These films are a candidate high refractive index mirror coating material to be used for future generation low temperature gravitational-wave detectors [46]. Ion-beam sputtering yields high density films with excellent optical properties. Although internal friction measurements have not been extended to the tunneling region and atomic density is generally not measured, a combination of efforts that includes elevated substrate temperatures and post-deposition heat treatment has resulted in improvements of Q^{-1} that has reached below 2×10^{-5} at temperatures around 10–20 K [43,45]. This is about the same as our lowest value of Q_0^{-1} deposited at 370°C and 431°C. It is interesting to note that, on one hand, a reduced deposition rate reduces both mechanical loss and optical absorption; and on the other hand, the lowest loss and absorption have been found in films deposited at a lower temperature (200°C) but being heat treated at 400–500°C [44]. This is consistent with our speculation that structural ordering afforded by surface diffusion is weakened by impingement disruptions during sputtering which makes post-deposition annealing most effective.

5. Conclusions

In this work, we systematically studied the substrate temperature dependence of low temperature internal friction, speed of sound, and shear modulus. It was hoped that the higher atomic density afforded by magnetron sputtering would help to further reduce the density of TLS from what has been achieved by *e*-beam evaporation. However, our results show sputtered *a*-Si has a higher TLS density at elevated substrate temperatures than those of *e*-beam. A detailed comparison with the results of *e*-beam *a*-Si shows that in spite of the high atomic density, the network connectivity in terms of speeds of sound and shear moduli fails to increase with T_{sub} as much as in *e*-beam *a*-Si. In fact, the effect of substrate temperature weakens substantially for sputtering, resulting in a higher density of TLS in sputtered *a*-Si than in *e*-beam at the highest substrate temperature although the opposite is true at room temperature. By comparing with previous annealing studies of sputtered *a*-Si and ion-implantation amorphized *a*-Si, we conclude that the different T_{sub} dependence between *e*-beam and sputtering originates from different film growth mechanisms. In *e*-beam evaporation, surface diffusion helps to coordinate surface adatoms to find low energy locations to improve structure order, and the effectiveness of such diffusion is enhanced with increasing T_{sub}. In sputtering, the relatively high energy of impinging ions tends to drive surface atoms into metastable locations resulting in higher atomic densities, and to dislocate the already coordinated surface atoms, which weakens the effect of surface diffusion afforded by high T_{sub}. The mechanical loss results of ion-beam sputtered *a*-Si are consistent with our observations. We conclude that a coordinated improvement of both atomic density and network connectivity toward their crystalline values is needed to eliminate TLS in *a*-Si. In spite of the disadvantage of sputtering revealed in this work, we hope that targeted tuning of sputtering parameters to reduce impinging ion energy, such as negative substrate bias, and to promote surface diffusion may help to alleviate the problem.

CRediT authorship contribution statement

Xiao Liu: Investigation, Conceptualization, Validation, Writing - original draft. **Matthew R. Abernathy:** Investigation, Validation. **Thomas H. Metcalf:** Investigation, Validation, Software. **Battogtokh Jugdersuren:** Investigation, Resources. **James C. Culbertson:** Investigation, Formal analysis. **Manel Molina-Ruiz:** Investigation, Validation. **Frances Hellman:** Supervision, Funding acquisition.

Declaration of competing interest

The authors declare that they have no known competing financial interests or personal relationships that could have appeared to influence the work reported in this paper.

Acknowledgments

This work is supported by the Office of Naval Research. We acknowledge the support of the NSF through the award DMR-1809498, and of the LSC Center for Coatings Research, jointly funded by the NSF and the Moore Foundation through Grant No. 6793.

References

[1] W. Phillips (Ed.), Amorphous Solids – Low Temperature Properties, Vol. 24 of Topics in Current Physics, Springer-Verlag, Berlin, Heidelberg, New York, 1981.
[2] P. Esquinazi (Ed.), Tunneling Systems in Amorphous and Crystalline Solids, Springer-Verlag, Berlin, Heidelberg, New York, 1998.
[3] R.C. Zeller, R.O. Pohl, Thermal conductivity and specific heat of noncrystalline solids, Phys. Rev. B 4 (1971) 2029–2041, https://doi.org/10.1103/PhysRevB.4.2029.
[4] P.W. Anderson, B.I. Halperin, C.M. Varma, Anomalous low-temperature thermal properties of glasses and spin glasses, Phil. Mag. 25 (1) (1972) 1–9, https://doi.org/10.1080/14786437208229210.
[5] W.A. Phillips, Tunneling states in amorphous solids, J. Low Temp. Phys. 7 (3) (1972) 351–360, https://doi.org/10.1007/BF00660072.
[6] L. Piché, R. Maynard, S. Hunklinger, J. Jäckle, Anomalous sound velocity in vitreous silica at very low temperatures, Phys. Rev. Lett. 32 (1974) 1426–1429, https://doi.org/10.1103/PhysRevLett.32.1426.
[7] M. von Schickfus, S. Hunklinger, L. Piché, Anomalous dielectric dispersion in glasses at low temperatures, Phys. Rev. Lett. 35 (13) (1975) 876–878, https://doi.org/10.1103/PhysRevLett.35.876.
[8] B. Golding, J. Graebner, R. Schutz, Intrinsic decay lengths of quasimonochromatic phonons in a glass below 1 K, Phys. Rev. B 14 (1976) 1660–1662, https://doi.org/10.1103/PhysRevB.14.1660.
[9] S. Hunklinger, W. Arnold, S. Stein, R. Nava, K. Dransfeld, Saturation of the ultrasonic absorption in vitreous silica at low temperatures, Phys. Lett. 42 (3) (1972) 253–255, https://doi.org/10.1016/0375-9601(72)90884-5.
[10] B. Golding, J. Graebner, B. Halperin, R. Schutz, Nonlinear phonon propagation in fused silica below 1 K, Phys. Rev. Lett. 30 (1973) 223–226, https://doi.org/10.1103/PhysRevLett.30.223.

[11] B. Golding, J.E. Graebner, Phonon echoes in glass, Phys. Rev. Lett. 37 (1976) 1105, https://doi.org/10.1103/PhysRevLett.37.1105.3. URL, https://link.aps.org/doi/10.1103/PhysRevLett.37.1105.3.

[12] J. Jäckle, L. Piché, W. Arnold, S. Hunklinger, Elastic effects of structural relaxation in glasses at low temperatures, J. Non-Cryst. Solids 20 (3) (1976) 365–391, https://doi.org/10.1016/0022-3093(76)90119-8.

[13] S. Hunklinger, W. Arnold, 3 - ultrasonic properties of glasses at low temperatures, in: of Physical Acoustics vol. 12, Academic Press, 1976, pp. 155–215, https://doi.org/10.1016/B978-0-12-477912-9.50008-4. URL, http://www.sciencedirect.com/science/article/pii/B9780124779129500084.

[14] G. Bellessa, Frequency and temperature dependence of the sound velocity in amorphous materials at low temperatures, Phys. Rev. Lett. 40 (1978) 1456–1459.

[15] B.E. White Jr., R.O. Pohl, Elastic properties of amorphous solids below 100 K, Z. Phys. B 100 (1996) 401–408, https://doi.org/10.1007/s002570050139.

[16] D. Tielbürger, R. Merz, R. Ehrenfels, S. Hunklinger, Thermally activated relaxation processes in vitreous silica: an investigation by brillouin scattering at high pressures, Phys. Rev. B 45 (1992) 2750–2760, https://doi.org/10.1103/PhysRevB.45.2750.

[17] R.O. Pohl, X. Liu, E. Thompson, Low-temperature thermal conductivity and acoustic attenuation in amorphous solids, Rev. Mod. Phys. 74 (2002) 991–1013, https://doi.org/10.1103/RevModPhys.74.991. URL, https://link.aps.org/doi/10.1103/RevModPhys.74.991.

[18] X. Liu, B.E. White Jr., R.O. Pohl, E. Iwanizcko, K.M. Jones, A.H. Mahan, B.N. Nelson, R.S. Crandall, S. Veprek, Amorphous solid without low energy excitations, Phys. Rev. Lett. 78 (1997) 4418–4421, https://doi.org/10.1103/PhysRevLett.78.4418. URL, https://link.aps.org/doi/10.1103/PhysRevLett.78.4418.

[19] X. Liu, D.M. Photiadis, H.-D. Wu, D.B. Chrisey, R.O. Pohl, R.S. Crandall, Disorder in tetrahedrally bonded amorphous solids, Phil. Mag. B 82 (2) (2002) 185–195, https://doi.org/10.1080/13642810208208541.

[20] D.R. Queen, X. Liu, J. Karel, T.H. Metcalf, F. Hellman, Excess specific heat in evaporated amorphous silicon, Phys. Rev. Lett. 110 (2013) 135901, https://doi.org/10.1103/PhysRevLett.110.135901. URL, https://link.aps.org/doi/10.1103/PhysRevLett.110.135901.

[21] X. Liu, D.R. Queen, T.H. Metcalf, J.E. Karel, F. Hellman, Hydrogen-free amorphous silicon with no tunneling states, Phys. Rev. Lett. 113 (2014), 025503, https://doi.org/10.1103/PhysRevLett.113.025503. URL, https://link.aps.org/doi/10.1103/PhysRevLett.113.025503.

[22] S. Swallen, K. Kearns, M. Mapes, Y. Kim, R. McMahon, M. Ediger, T. Wu, L. Yu, S. Satija, Organic glasses with exceptional thermodynamic and kinetic stability, Science 315 (5810) (2007) 353–356, https://doi.org/10.1126/science.1135795.

[23] T. Pérez-Castañeda, C. Rodríguez-Tinoco, J. Rodríguez-Viejo, M. Ramos, Suppression of tunneling two-level systems in ultrastable glasses of indomethacin, Proc. Natl. Acad. Sci. U. S. A 111 (31) (2014) 11275–11280, https://doi.org/10.1073/pnas.1405545111.

[24] D. Queen, X. Liu, J. Karel, H. Jacks, T. Metcalf, F. Hellman, Two-level systems in evaporated amorphous silicon, J. Non-Cryst. Solids 426 (2015) 19–24, https://doi.org/10.1016/j.jnoncrysol.2015.06.020.

[25] M. Von Haumeder, U. Strom, S. Hunklinger, Acoustic anomalies in amorphous thin films of si and sio_2, Phys. Rev. Lett. 44 (1980) 84–87, https://doi.org/10.1103/PhysRevLett.44.84. URL, https://link.aps.org/doi/10.1103/PhysRevLett.44.84.

[26] J. Duquesne, G. Bellessa, Rayleigh waves in amorphous germanium at low temperature: evidence for the existence of tunneling defects, J. Phys. C Solid State Phys. 16 (3) (1983) L65–L68, https://doi.org/10.1088/0022-3719/16/3/003.

[27] R. van den Berg, H. von Löhneysen, H.J. Schink, Calorimetric investigation of a-Si and a-Ge in high magnetic fields, J. Non-Cryst. Solids 77 & 78 (1985) 1339, https://doi.org/10.1016/0022-3093(85)90905-6.

[28] X. Liu, R.O. Pohl, Low-energy excitations in amorphous films of silicon and germanium, Phys. Rev. B 58 (1998) 9067–9081.

[29] C. Müller, J.H. Cole, J. Lisenfeld, Towards understanding two-level-systems in amorphous solids: insights from quantum circuits, Rep. Prog. Phys. 82 (12) (2019) 124501, https://doi.org/10.1088/1361-6633/ab3a7e.

[30] K. Craig, J. Steinlechner, P.G. Murray, A.S. Bell, R. Birney, K. Haughian, J. Hough, I. MacLaren, S. Penn, S. Reid, R. Robie, S. Rowan, I.W. Martin, Mirror coating solution for the cryogenic einstein telescope, Phys. Rev. Lett. 122 (2019) 231102, https://doi.org/10.1103/PhysRevLett.122.231102. URL, https://link.aps.org/doi/10.1103/PhysRevLett.122.231102.

[31] P. Medwick, B. White Jr., R. Pohl, Elastic properties of amorphous and crystalline $B_{1-x}C_x$ and boron at low temperatures, J. Alloys Compd. 270 (1) (1998) 1–15, https://doi.org/10.1016/S0925-8388(98)00119-4.

[32] T.H. Metcalf, X. Liu, M.R. Abernathy, Improving the mechanical quality factor of ultra-low-loss silicon resonators, J. Appl. Phys. 123 (23) (2018) 235105, https://doi.org/10.1063/1.5027486.

[33] B.H. Houston, D.M. Photiadis, M.H. Marcus, J.A. Bucaro, X. Liu, J.F. Vignola, Thermoelastic loss in microscale oscillators, Appl. Phys. Lett. 80 (7) (2002) 1300–1302, https://doi.org/10.1063/1.1449534.

[34] A. Fefferman, A. Maldonado, E. Collin, X. Liu, T. Metcalf, G. Jernigan, Elastic measurements of amorphous silicon films at mk temperatures, J. Low Temp. Phys. 187 (5) (2017) 654–660, https://doi.org/10.1007/s10909-016-1686-6.

[35] M. Hopcroft, W. Nix, T. Kenny, What is the young's modulus of silicon? J. Microelectromech. Syst. 19 (2) (2010) 229–238, https://doi.org/10.1109/JMEMS.2009.2039697.

[36] J.S. Custer, M.O. Thompson, D.C. Jacobson, J.M. Poate, S. Roorda, W.C. Sinke, F. Spaepen, Density of amorphous si, Appl. Phys. Lett. 64 (4) (1994) 437–439, https://doi.org/10.1063/1.111121.

[37] I.R. Cox-Smith, H.C. Liang, R.O. Dillon, Sound velocity in amorphous films of germanium and silicon, J. Vac. Sci. Technol. 3 (3) (1985) 674–677, https://doi.org/10.1116/1.573278.

[38] R. Vacher, H. Sussner, M. Schmidt, Attenuation of surface phonons in opaque materials measured by Brillouin-scattering, Solid State Commun. 34 (5) (1980) 279–281, https://doi.org/10.1016/0038-1098(80)90557-8}.

[39] M. Molina-Ruiz, Y.J. Rosen, H.C. Jacks, M.R. Abernathy, T.H. Metcalf, X. Liu, J.L. Dubois, F. Hellman, Origin of Mechanical and Dielectric Losses from Two-Level Systems in Amorphous Silicon, 2020 arXiv:arXiv:2008.07489.

[40] M. Molina-Ruiz, H.C. Jacks, D.R. Queen, Q. Wang, R.S. Crandall, F. Hellman, Two-level systems and growth-induced metastability in hydrogenated amorphous silicon, Mater. Res. Express 7 (9) (2020), 095201, https://doi.org/10.1088/2053-1591/abb498.

[41] L. Berthier, P. Charbonneau, E. Flenner, F. Zamponi, Origin of ultrastability in vapor-deposited glasses, Phys. Rev. Lett. 119 (2017) 188002, https://doi.org/10.1103/PhysRevLett.119.188002. URL, https://link.aps.org/doi/10.1103/PhysRevLett.119.188002.

[42] F. Dheurle, J. Harper, Note on the origin of intrinsic stresses in films deposited via evaporation and sputtering, Thin Solid Films 171 (1) (1989) 81–92, https://doi.org/10.1016/0040-6090(89)90035-7}.

[43] P.G. Murray, I.W. Martin, K. Craig, J. Hough, R. Robie, S. Rowan, M.R. Abernathy, T. Pershing, S. Penn, Ion-beam sputtered amorphous silicon films for cryogenic precision measurement systems, Phys. Rev. D 92 (2015), 062001, https://doi.org/10.1103/PhysRevD.92.062001. URL, https://link.aps.org/doi/10.1103/PhysRevD.92.062001.

[44] R. Birney, J. Steinlechner, Z. Tornasi, S. MacFoy, D. Vine, A.S. Bell, D. Gibson, J. Hough, S. Rowan, P. Sortais, S. Sproules, S. Tait, I.W. Martin, S. Reid, Amorphous silicon with extremely low absorption: beating thermal noise in gravitational astronomy, Phys. Rev. Lett. 121 (2018) 191101, https://doi.org/10.1103/PhysRevLett.121.191101. URL, https://link.aps.org/doi/10.1103/PhysRevLett.121.191101.

[45] J. Steinlechner, I.W. Martin, A.S. Bell, J. Hough, M. Fletcher, P.G. Murray, R. Robie, S. Rowan, R. Schnabel, Silicon-based optical mirror coatings for ultrahigh precision metrology and sensing, Phys. Rev. Lett. 120 (2018) 263602, https://doi.org/10.1103/PhysRevLett.120.263602. URL, https://link.aps.org/doi/10.1103/PhysRevLett.120.263602.

[46] R.X. Adhikari, O. Aguiar, K. Arai, B. Barr, R. Bassiri, G. Billingsley, R. Birney, D. Blair, J. Briggs, A.F. Brooks, D.D. Brown, H.-T. Cao, M. Constancio, S. Cooper, T. Corbitt, D. Coyne, E. Daw, J. Eichholz, M. Fejer, A. Freise, V. Frolov, S. Gras, A. Green, H. Grote, E.K. Gustafson, E.D. Hall, G. Hammond, J. Harms, G. Harry, K. Haughian, F. Hellman, J.-S. Hennig, M. Hennig, S. Hild, W. Johnson, B. Kamai, D. Kapasi, K. Komori, M. Korobko, K. Kuns, B. Lantz, S. Leavey, F. Magana-Sandoval, A. Markosyan, I. Martin, R. Martin, D.V. Martynov, D. Mcclelland, G. Mcghee, J. Mills, V. Mitrofanov, M. Molina-Ruiz, C. Mow-Lowry, P. Murray, S. Ng, L. Prokhorov, V. Quetschke, S. Reid, D. Reitze, J. Richardson, R. Robie, I. Romero-Shaw, S. Rowan, R. Schnabel, M. Schneewind, B. Shapiro, D. Shoemaker, B. Slagmolen, J. Smith, J. Steinlechner, S. Tait, D. Tanner, C. Torrie, J. Vanheijningen, P. Veitch, G. Wallace, P. Wessels, B. Willke, C. Wipf, H. Yamamoto, C. Zhao, L. Barsotti, R. Ward, A. Bell, R. Byer, A. Wade, W.Z. Korth, F. Seifert, N. Smith, D. Koptsov, Z. Tornasi, A. Markowitz, G. Mansell, T. Mcrae, P. Altin, M.J. Yap, M. Van Veggel, G. Eddolls, E. Bonilla, E.C. Ferreira, A.S. Silva, M.A. Okada, D. Taira, D. Heinert, J. Hough, K. Strain, A. Cumming, R. Route, D. Shaddock, M. Evans, R. Weiss, A Cryogenic Silicon Interferometer for Gravitational-Wave Detection, arXiv e-prints, 2020. arXiv:2001.11173arXiv:2001.11173.